American Mineralogist, Volume 92, pages 1856–1861, 2007

Direct EXAFS evidence for incorporation of As^{5+} in the tetrahedral site of natural andraditic garnet

J.M. Charnock,[1] D.A. Polya,[2] A.G. Gault,[2] and R.A. Wogelius[2,*]

[1]CCLRC Daresbury Laboratory, Daresbury, Warrington, WA4 4AD, U.K.
[2]School of Earth, Atmospheric and Environmental Sciences and Williamson Research Centre for Molecular Environmental Science, The University of Manchester, M13 9PL U.K.

Abstract

Exceptionally high-quality X-ray absorption spectroscopy (XAS) spectra of the As *K*-edge measured on a garnet from the Central Oslo Rift (Jamtveit et al. 1993) are presented and interpreted. The best fit to the extended X-ray absorption fine structure (EXAFS) spectrum indicates that arsenic occurs predominantly as As^{5+} in the tetrahedral Si^{4+} site. The first shell As-O bond lengths of 1.69 Å are identical to those observed for As^{5+}-O in sodium arsenate and the edge position of 11872 eV is also characteristic of As^{5+}. Determination of oxidized As within the structure places an important constraint on fluid chemistry, but perhaps even more importantly, EXAFS fitting of outer shells (As-Ca 3.07, 3.75, 5.71, 6.11 Å; As-Fe/Al 3.47, 5.35 Å; As-Si 3.88, 5.60, 5.91 Å) in this high-quality data set gives unequivocal evidence that AsO_4^{3-} substitutes for SiO_4^{4-} in the garnet tetrahedral site. This is, to the best of our knowledge, the first such XAS study yielding direct evidence, through outer shell fitting, for both the coordination environment and oxidation state of arsenic within (as opposed to sorbed onto) a silicate mineral.

Keywords: Arsenic, garnet, XAS, EXAFS, oxidation state, coordination

Introduction

Despite extensive interest, reflected in numerous X-ray absorption spectroscopy (XAS) studies of the solid phase speciation of arsenic (Morin and Calas 2006; Coker et al. 2006; Pascua et al. 2005; Cances et al. 2005; Savage et al. 2005; Thoral et al. 2005; Sherman and Randall 2003; Bostick and Fendorf 2003; Tournassat et al. 2002; Farquhar et al. 2002), there is a paucity of XAS data on the oxidation state and especially the coordination environment of arsenic in, as opposed to sorbed onto, silicate minerals. Such data are potentially invaluable to the interpretation of XAS spectra of soils and sediments in which arsenic may occur either within the bulk structure or sorbed onto several different phases as a range of different surface complexes, each with As in a unique coordination environment (Rowland et al. 2005; Gault et al. 2003a, 2003b, 2005; Hudson-Edwards et al. 2005; Paktunc et al. 2003, 2004; Morin et al. 2003; La Force et al. 2000).

As^{5+} substitution for tetrahedral silica in silicate minerals was postulated over 40 years ago (Esson et al. 1965) as one of several ways to explain the presence of trace arsenic in sulfide-poor rocks, but previously this coordination environment for As has never been directly observed via XAS. The paucity in data stems from the fact that arsenic is a major component of only a small number of mostly unusual silicate minerals. These include medaite, $(Mn,Ca)_6(V,As)Si_5O_{18}(OH)$ (Gramaccioli et al. 1981), and ardennite, $(Mn,Ca,Mg)_4(Al,Mg,Fe)_6(V,As)Si_5O_{22}(OH)_6$ (Donnay and Allmann 1968), where As^{5+} substitutes for V^{5+} in a tetrahedral site in both structures, and filatovite, $K[(Al,Zn)_2(As,Si)_2O_8]$ (Filatov et al. 2004), in which As^{5+} substitutes for Si^{4+} and in which $(As,Si)O_4$ tetrahedra are surrounded by $(Al,Zn)O_4$ tetrahedra and vice versa. Incorporation of As^{5+} into the feldspar-like tetrahedral framework is possible as charge is balanced through the incorporation of Zn^{2+} or Al^{3+} into adjacent tetrahedral sites.

Only recently has the oxidation state of arsenic in a small number of silicate minerals been determined, but problems with data quality due to the extremely low concentrations of As have hindered the determination of the full coordination environment. Pascua et al. (2005) obtained first shell information, showing that most (~70 to 90%) of the arsenic present in hydrothermally precipitated phases from northwestern Japan was As^{3+}. As^{5+} was indeed also found to be present and was postulated to be incorporated into amorphous silica and perhaps into the smectite stevensite, but the mode of incorporation of oxidized As^{5+} could not be unambiguously determined. Hattori et al. (2005) analyzed As in forearc mantle serpentinites and found most to be present as oxidized As^{5+}, with As^{5+} representing over 80% of the arsenic inventory in some samples. They concluded that at least some of this As^{5+} was likely to be structurally incorporated within antigorite, substituting for Si^{4+} and maintaining charge balance via a coupled substitution of the form:

$$Al^{3+} + As^{5+} \leftrightarrow 2\ Si^{4+}.$$

Neither study was able to obtain information beyond the first shell and so assignment of As^{5+} to the tetrahedral site, although likely, was not directly determined. Indeed, Hattori et al. (2005) reported a coordination number for arsenic of 5.2; but of course with As concentrations as low as 6 ppm it is understandable that spectra were difficult to interpret. Therefore, it is clear that analy-

* E-mail: Roy.Wogelius@manchester.ac.uk

sis of natural silicates with higher As concentrations is needed to understand the partitioning behaviour between arsenic-bearing geochemical fluids and silicate minerals.

In this study, we present XAS spectra of an arsenic-rich skarn garnet sampled from the Central Oslo Rift (Jamtveit et al. 1993). Skarn garnets are formed during contact metamorphism-driven hydrothermal alteration of carbonate rocks and often show strong zoning with respect to major and minor elements. Samples from the Central Oslo Rift containing exceptionally high levels of arsenic (2500 ppm) and tungsten (600 ppm) have been previously studied using microPIXE and exhibit strong zoning in As and W, interpreted as reflecting a sudden change in the growth conditions (Jamtveit et al. 1993; Grime et al. 1993). In this case arsenic-bearing andraditic garnet has overgrown more grossular-rich cores. It was postulated that the andradite overgrowths were produced via boiling reactions in hydrothermal fluids in contact with the Drammen granite (Jamtveit et al. 1993). Boiling enriched the fluid in As and W, created an oxidized fluid, and escape of this fluid led to rapid precipitation of Fe^{3+}-rich and trace element enriched garnet. Several fluid pulses are apparently recorded in the garnet zones. Crystallographic analysis of garnet texture indicates that growth rates decreased as a function of time and this is correlated with a fairly rapid decrease in average As concentrations through the andraditic portion of the garnet. Postulation of oxidizing conditions during garnet growth is petrologically reasonable, based upon the thermodynamic data for the reaction hedenbergite + O_2 (g) ↔ andradite + magnetite + quartz of Zhang and Saxena (1991), as the garnet samples were taken from a magnetite mine where the garnet and magnetite are co-precipitates (Jamtveit et al. 1993). We have collected X-ray absorption spectroscopy data to elucidate the site occupied by the arsenic in one of these samples. We also note that more recently skarn garnets zoned in arsenic (up to 150 ppm) have also been identified within the Connemara area of western Ireland (Wogelius, unpub. data).

Experimental methods

A polycrystalline aggregate sample with a mass of approximately 50 g was used in this study. Powders were produced by visually inspecting the sample and chipping off garnet fragments while avoiding obvious impurities. These fragments were then ground with an agate mortar and pestle for XAS, X-ray diffraction (XRD), and attenuated total reflectance-Fourier transform infrared (ATR-FTIR) analysis. A standard petrographic thin section was also prepared from a large fragment for electron microprobe analysis.

Arsenic *K*-edge XAS spectra were collected on Station 16.5 at the Daresbury Council for the Central Laboratories of the Research Councils, Synchrotron Radiation Source (CCLRC SRS) operating at 2 GeV with an average current of 140 mA, using a vertically focusing mirror and a sagitally bent focussing Si(220) double crystal monochromator detuned to 70% transmission to minimize harmonic contamination. The fine powder sample was mounted in an aluminium sample cell using Sellotape windows. Fluorescence spectra were collected at liquid nitrogen temperature using an Ortec 30-element solid-state Ge detector. Eight scans were collected and averaged to improve the signal to noise ratio. The spectrum of a sample of sodium arsenate, placed behind the garnet sample and shielded with lead from the fluorescence detector, was collected simultaneously in transmission mode to provide an internal calibration and ensure that the edge position was measured accurately. Transmission spectra of three standard compounds (sodium arsenate, sodium arsenite, and arsenopyrite) were also collected at room temperature for comparison.

The background subtracted extended X-ray absorption fine structure (EXAFS) spectrum was analyzed in EXCURV98 using full curved-wave theory (Binsted 1998; Gurman et al. 1984). Phase shifts were derived in the program from ab initio calculations using the program defaults in EXCURV98, which assumes a sodium chloride structure (octahedral geometry) for each absorber-scatterer pair. Hedin-Lundqvist potentials and von Barth ground states (Hedin and Lundqvist 1969) were used. The data were fitted by defining a theoretical model and comparing the calculated EXAFS spectrum with the experimental data. Shells of backscatterers were added around the arsenic and, by refining (1) an energy correction E_f (the Fermi energy); (2) the absorber-scatterer distance; and (3) the Debye-Waller factor for each shell, a least squares residual [the *R*-factor (Binsted et al. 1992)] was minimized. Essentially, for each shell of scatterers in the fit there were two free parameters refined, the absorber-scatterer distance and the Debye-Waller factors; a single parameter was refined for the edge-energy shift correction. The number of atoms in each shell was chosen from the known garnet crystal structure, using either the tetrahedral Si site, or the octahedral Al/Fe site.

XRD scans were completed on a Philips PW1730; scans ran from 10 to 70 °2θ with a step size of 0.02° and analysis time of 1 s per step. Silicon was used as an internal standard to ensure accuracy of measured peak positions. Data analysis was completed using the Bruker EVA software.

Electron microprobe analysis was performed using a Cameca SX100 with 5 wavelength dispersive spectrometers. Analytical conditions were 15 kV accelerating voltage and 20 nA beam current. GaAs was used as the arsenic standard, other standards were as follows: W-scheelite, Fe-fayalite, Mn-tephroite, Ca-wollastonite, Ti-rutile, Si-wollastonite, Al-corundum, and Mg-periclase. Point analyses were completed to verify the presence of As, and then a set of points with 5 µm spacing along a line 310 µm long from rim to core intersecting many different growth zones was analyzed. Count times were 100 s for As and W, 20 s for all other elements. The limits of detection for As and W in this set-up were approximately 0.015 at. wt% As (0.06 oxide wt% As_2O_5) and 0.02 at. wt% W (0.03 oxide wt% WO_3). Data were corrected using the Cameca PAP method.

ATR-FTIR-A Biorad FTS 6000 spectrometer equipped with a deuterated triglycine sulfate (DTGS) detector was used with an ATR attachment. All spectra were a sum of 16 scans collected using non-polarised light at a resolution of 4 cm^{-1}. Background was collected from the ATR attachment while empty. Background subtraction and data analysis were completed using Win-IR Pro software.

Results

XAS

Figure 1 compares the X-ray absorption near edge structure (XANES) spectrum of the garnet to several reference compounds. Along with the XANES spectrum the full EXAFS spectrum was measured, allowing precise bond distances and coordination numbers for arsenic in this garnet to be determined. The EXAFS data (solid line) and fit (broken line) are presented in Figure 2. The associated radial distribution functions (Fourier transform of the EXAFS phase shifted for As-O) of the data and best fit are shown in Figure 3 (symbols same as previous). The EXAFS oscillations giving rise to the features seen in the Fourier transform at ca. 4.4 Å were not fitted—they are probably due to the oxygen shells at 4.106 and 4.371 Å in the crystal structure, but adding oxygen scatterers at these distances did not significantly improve the residual.

It is clear that the near-edge structure of the garnet spectrum corresponds in energy (11872 eV) and shape to the sodium arsenate standard spectrum, indicating that the arsenic in the garnet is As^{5+} and that it is surrounded by oxygen atoms in its inner coordination sphere. Furthermore the best fit to the EXAFS spectrum indicated that, in contrast to the previously supposed occurrence of arsenic as As^{3+} in the Al/Fe^{3+} octahedral site (Grime et al. 1993), arsenic occurred predominantly as As^{5+} in the tetrahedral Si^{4+} site. Table 1 presents the full details of the radial distribution functions for the structure of $Ca_3Al_{1.6}Fe_{0.4}Si_3O_{12}$ grossular garnet (left hand side of the table; Takeuchi et al. 1982) with the results of the EXAFS fitting for arsenic in this garnet (right hand side of the table).

First let us consider the inner shell of absorbers. The As-O bond length of 1.69 Å in the unknown is identical to that observed

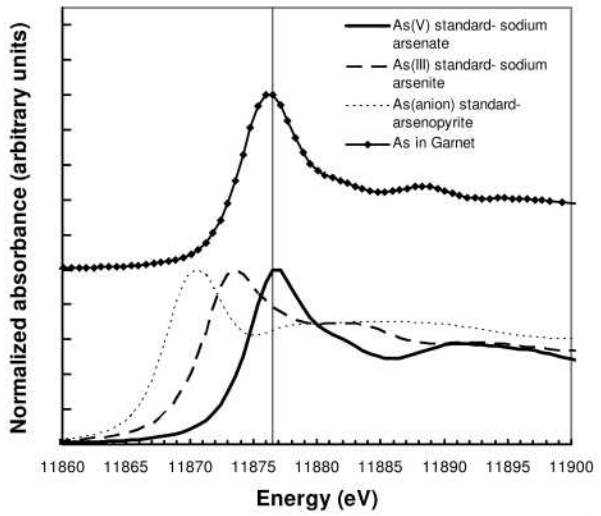

FIGURE 1. Comparison of As *K*-edge XANES spectra from three model compounds (arsenopyrite, sodium arsenite, sodium arsenate) to the andraditic garnet. The garnet spectrum is completely different from either arsenopyrite or sodium arsenite. Furthermore, note that the edge position for As in the garnet is identical with the sodium arsenate standard (vertical line added for reference), indicating all or nearly all is present as As^{5+} in the unknown.

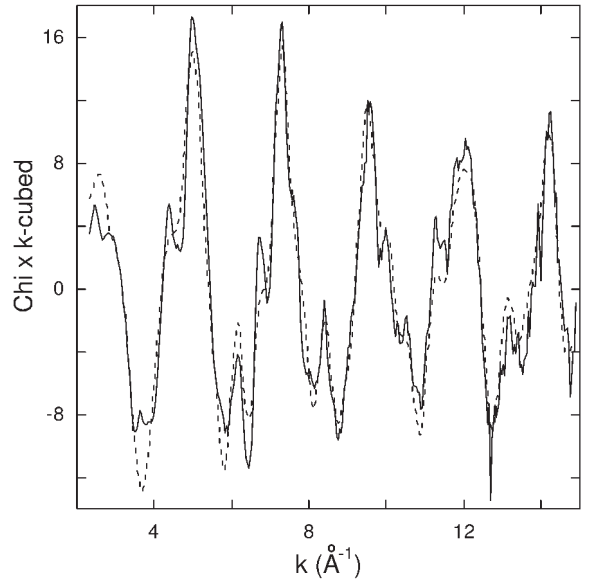

FIGURE 2. As *K*-edge EXAFS (solid line) and theoretical fit (broken line) of the garnet sample.

for As^{5+}-O in sodium arsenate. The type and number of nearest neighbors extracted from the EXAFS analysis is also consistent with tetrahedral oxygen coordination. The bond distances for this inner shell are totally inconsistent with the octahedral oxygen distances of 1.938 Å. Next, we may consider the second shell, which produces a high amplitude peak in the radial distribution function at 3.07 Å. This can be fit with two Ca atoms in this shell very closely matching the theoretical distance of 2.968 Å for two Ca atoms from the center of the tetrahedral site, but is

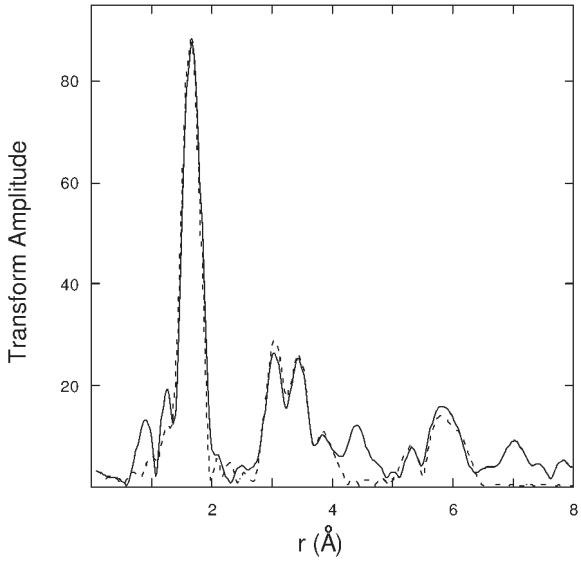

FIGURE 3. Radial distribution function (Fourier transform) of the garnet EXAFS spectrum (solid line) and fit (broken line) as presented in Figure 2. Parameters used to generate this fit are given in Table 1.

a poor match for the 6 Ca atoms, which sit at 3.318 Å distance from the center of the octahedral site. Similarly, the next highest amplitude feature, at 3.47 Å in the radial distribution function, can be matched with 4 Fe or Al scatterers at that distance, in relatively good agreement with the theoretical occupancy and distance for tetrahedral coordination. Seven more shells of scatterers may be added out to 6.11 Å distance from the central absorber, all of which significantly improve the fit to the EXAFS data and all of which are wholly consistent with tetrahedral coordination of the central absorber in terms of bond distance, number of scatterers, and type of scatterer. (Past the first shell the O atoms are not included in the EXAFS fitting because of their low electron density and minimal effect on scattering at long distance.) Without question these data show that As^{5+} substitutes for Si^{4+} in the tetrahedral site.

Electron microprobe

To check the bulk composition of the garnet a standard petrographic thin section was prepared. Approximately 15% of the thin section was magnetite, with void space approximately 5%. A large garnet, 1.5 mm in diameter, was analyzed by point-scanning along a line from rim toward the core. The back-scattered image showed clear oscillatory zonation as seen in several other studies of these garnets (Jamtveit 1991; Jamtveit et al. 1993). Table 2 shows some selected point analyses. These results are nearly identical to previously published analyses and corroborate that the arsenic is indeed held within the garnet structure, with arsenic zoning following zoning in other elements. Note in particular that the highest tungsten and arsenic concentrations occur together at point 14. Positive correlation of these two trace elements has already been documented (Jamtveit et al. 1993). The best technique for quantifying the As concentration in these samples is PIXE (proton induced X-ray emission) because the background levels produced in EMA result in a relatively high limit of detection for As, however PIXE has virtually no

TABLE 1. Comparison of the radial distribution functions for the structure of $Ca_3Al_{1.6}Fe_{0.4}Si_3O_{12}$ grossular garnet (Takeuchi et al. 1982) to the results of the EXAFS fitting

Crystal structure radial distributions						EXAFS analysis, *R*-factor = 28.9			
Al/Fe site			Si site						
N	Type	*r* (Å)	N	Type	*r* (Å)	N	Type	*r* (Å)	$2\sigma^2$ (Å^2)
			4	O	1.648	4	O	1.69†	0.003§
6	O	1.938							
			2	Ca	2.968	2	Ca	3.07‡	0.004
			4	O	3.229				
6	Ca	3.318	4	Al/Fe	3.318	4	Fe*	3.47	0.010
6	Si	3.318							
			4	O	3.560				
			4	O	3.617				
			4	Ca	3.635	4	Ca	3.75	0.012
			4	Si	3.635	4	Si	3.88	0.030
6	O	3.677							
6	O	4.195	4	O	4.106				
6	O	4.475	4	O	4.371				
6	O	5.045	4	O	5.075				
6	Al/Fe	5.141							
			4	O	5.246				
6	Ca	5.351	4	Al/Fe	5.351	4	Fe*	5.35	0.010
6	Si	5.351							
			4	O	5.449				
			4	O	5.497				
			8	Ca	5.553	8	Ca	5.71	0.010
			8	Si	5.553	8	Si	5.60	0.010
6	O	5.699							
6	O	5.794	4	O	5.844				
6	O	5.909	4	O	5.879				
6	Al/Fe	5.936	4	Ca	5.936	4	Ca	6.11	0.012
			2	Si	5.936	2	Si	5.91	0.020

Note: Fe* = this site could be fitted using Al or Fe scatterers, or a mixture.
Errors: *r* is ±0.02 Å for the first shell (†), ±0.05 Å for outer shells (‡), and $2\sigma^2$ is ±25% (§).

TABLE 2. Electron microprobe analysis

	Pt. 1 Rim 0 μm*	Pt. 14 60 μm	Pt. 30 155 μm	Pt. 60 Core 310 μm
As_2O_5 (±0.06)	bdl	0.160	0.070	bdl
WO_3 (±0.06)	bdl	0.092	0.065	bdl
Fe_2O_3 (±0.25)	22.595	26.813	22.286	22.881
MnO (±0.05)	0.773	0.532	0.713	0.651
CaO (±0.08)	34.327	34.394	34.660	34.574
TiO_2 (±0.01)	0.011	0.028	0.021	0.026
SiO_2 (±0.07)	35.690	35.406	35.974	36.008
Al_2O_3 (±0.03)	6.224	2.608	6.165	5.956
MgO (±0.01)	0.017	0.036	0.022	0.021
Total	99.688	100.069	99.976	100.117

Note: bdl = below detection limit.
* Distances indicate position relative to the first point analysis taken at the outer rim of the crystal.

TABLE 3. Garnet XRD analysis

Garnet sample		Reference patterns		
d-spacing (Å)	Intensity	*d*-spacing (Å)	Intensity	Pattern
4.239	10	4.190	1	39–368*
3.363	14	3.360	70	2–1124†
2.995	81	2.962	35	39–368
2.678	100	2.650	100	"
2.551	9	2.571	14	10–288‡
2.530	14	2.526	7	39–368
2.444	45	2.418	18	"
2.347	21	2.323	16	"
2.186	20	2.202	18	10–288
2.163	5	2.163	12	39–368
2.095	6	2.094	3	"
2.017	6	2.030	100	2–1124
1.941	24	1.922	18	39–368
1.893	7	1.874	2	"
1.731	15	1.710	12	"
1.659	29	1.643	18	"
1.599	50	1.584	30	"
1.496	12	1.481	6	"

Note: Ref. patterns are from the Powder Diffraction File Release 1999, Data Sets 1–49 and 70–86.
* Grossular.
† Hydrogrossular.
‡ Synthetic andradite.

background at the As*K*α emission line and therefore the limit of detection may be below 1 ppm. However, the EMA analyses of this sample do show As levels ranging from the detection limit to 0.16 oxide wt% (150–1200 ppm), in complete agreement with PIXE measurements that showed concentrations to vary between 70–2500 ppm (Jamtveit et al. 1993). This gives us confidence that the arsenic XAS results from this sample are indeed produced by As in garnet and not from any other phase.

X-ray diffraction

Impurities within the bulk sample, as discussed in the electron microprobe analysis above, were avoided when fragments were taken for powder measurements using XRD, XAS, and FTIR. We note that standard XRD has a limit of detection of approximately 5% by volume. In any case we completed analysis of powdered garnet as used in the XAS experiments. Table 3 shows the XRD results. This garnet is a solid solution andradite-grossular garnet and therefore none of the standard reference patterns are a perfect fit. However, almost all of the intense peaks are nicely bracketed by the two end-member reference pattern peak locations for grossular and andradite. Two additional peaks are present, however, at *d*-spacings of 3.363 and 2.017 Å. These are the two most intense peaks for the hydrogrossular reference pattern, and we suggest it is likely that portions of the garnet may have sufficient hydroxyl incorporated into the structure to result in the presence of these additional peaks. FTIR analysis presented below corroborates this inference. Perhaps more importantly however, Table 4 presents the most intense diffraction peaks for impurities that would be likely hosts for arsenic and do not overlap with garnet peaks. None of these peaks appear in the garnet pattern and therefore we are confident that by optically selecting fragments for powder analysis we are able to avoid impurities successfully. We also note that besides magnetite none of these phases have been identified in these samples by any other means. As discussed below, the XAS analysis is diagnostic in any case.

ATR-FTIR

To assess whether hydrogen had been structurally incorporated into the garnet structure as hydroxyl ATR-FTIR was completed on a powder sample prepared similarly to those used in XAS and XRD. The ATR-FTIR measurement is shown in Figure 4. In Figure 4a, we show the full spectrum and that our detector is well calibrated because the CO_2 peak is exactly where it should be theoretically. (Based on preliminary FTIR imaging results we infer that the strength of this CO_2 peak is caused in large part by inclusions within the solids and is not solely due to atmospheric contamination. In contrast a broad band corresponding to molecular water is not observed.) Therefore if we consider detector resolution and perhaps the possibility that only slight miscalibration is allowed, then we may conclude that the peak positions are accurate to within, at worst, ±10 cm^{-1}. Below, in Figure 4b we highlight the clear absorption band structure in the region typically ascribed to –OH stretch in silicate minerals, with at least four bands identified at 3730, 3700, 3627, and 3599

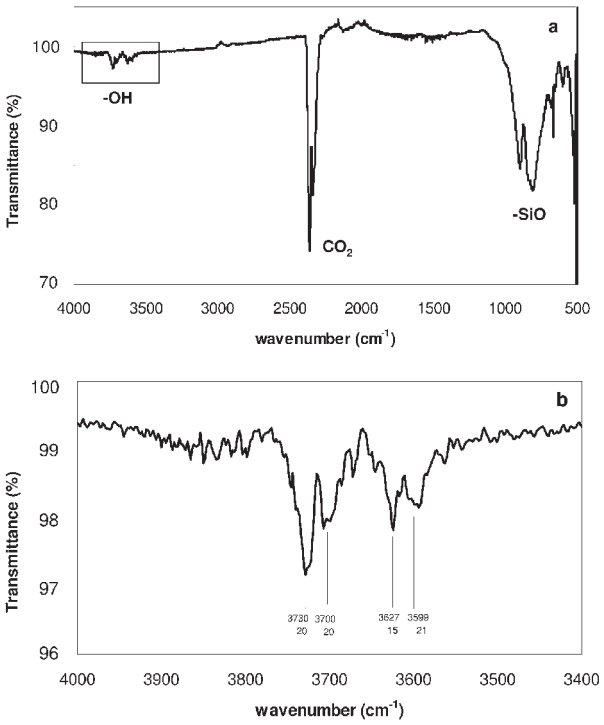

FIGURE 4. ATR-FTIR transmission spectra of garnet powder. (**a**) Full spectrum showing all features; boxed area labeled as –OH is expanded in the second panel. (**b**) Selected region highlighting the presence of –OH absorption bands. At least four are present at 3730, 3700, 3627, and 3599 cm^{-1}. FWHM for each peak is shown below the band label.

cm^{-1}. The second most intense peak at 3627 cm^{-1} and the associated shoulder peak at 3599 cm^{-1} can be compared to absorption bands associated with either hydrous grossular or andradite garnets (Rossman and Aines 1991; Amthauer and Rossman 1998). Given the estimated errors, the peak at 3700 may be similar to previously reported peaks in the vicinity of 3690 cm^{-1} for hydrous grossular (Rossman and Aines 1991), and the peak at 3730 cm^{-1} may be analogous to the low intensity but distinct peak determined at 3738 cm^{-1} for hydroandradite (Amthauer and Rossman 1998). Rossman and Aines (1991) clearly show that the IR absorption due to incorporated OH groups in grossular garnets is extremely complicated, and that even seven different classes of IR behavior are not sufficient to describe observed natural samples. It is beyond the scope of this paper to fully quantify the FTIR spectra, however the data presented indicate that hydroxyl is definitely present and at least in part substitutes into the tetrahedral site for silicon. Based on the relatively low intensity of the absorption in the hydroxyl region (approximately 3%) we estimate the weight percent of H_2O in this garnet sample to be below 1%, on the order of 0.10 to 0.20 wt%.

DISCUSSION

The determination that all of the arsenic present in this sample is As^{5+} is useful because it is consistent with other petrologic indications that the fluids in this system were relatively oxidized. Hattori et al. (2005) also use the presence of As^{5+} to constrain redox conditions in serpentinites. Recognizing the possibility that redox sensitive As^{5+} substitutes into silicates may improve our ability to constrain the oxidation state of several other hydrothermal systems.

TABLE 4. Intense diffraction peaks of potential impurities

Reference patterns	*d*-spacing (Å)	Intensity
Arsenopyrite (43–1470)	2.4208	70
	2.4082	67
Magnetite (25–1376)	2.51	100
Hematite (33–0664)	2.519	70
	3.684	30
Ferrihydrite (46–1315)	1.88	100

Note: Ref. patterns are from the Powder Diffraction File Release 1999, Data Sets 1–49 and 70–86.

Still open, however, is the question of how charge balance is maintained. From the arsenic XAS data alone it is not possible to definitively explain how charge balance is maintained within the structure; however it is clear that either a defect or coupled substitution must occur. Iron and As concentrations vary sympathetically in the garnet zoning profiles, hence it is possible that an $Fe^{3+} + As^{5+}$ substitution for 2 Si^{4+} may occur. A similar coupled $Al^{3+} + As^{5+}$ for 2 Si^{4+} substitution is theoretically possible as suggested by Hattori et al. (2005), although in this garnet Al and As concentrations are anti-correlated, and hence in this case this mechanism is unlikely. Our preferred mechanism to explain charge balance incorporates both what we know about the crystallization kinetics of these garnets and their full stoichiometries.

As fully discussed in Jamtveit et al. (1993), the As-rich garnet analyzed here is an andradite-rich overgrowth on a grossular-rich core. The sharp chemical zoning seen for As incorporation is also reflected in the major element chemistry; however not only do Fe concentrations increase at this front, but Si and Al levels decrease significantly as well. In fact, significant quantities of hydroxyl are postulated for some analyses to maintain charge balance in the overgrowth, with all charge on 1 of 12 O atoms compensated by protons. This "hydrogarnet" composition is reasonable given that the growth kinetics were rapid in the overgrowth, with the growing crystal able to substitute As^{5+} and protons into the tetrahedral site from a fluid relatively enriched in these components. Both the precipitation rate and As concentrations apparently decrease as the reaction proceeds, consistent with this interpretation. We furthermore note that the neutral aqueous species of As^{5+} is H_3AsO_4, which carries exactly the amount of positive charge needed to balance the loss of two silica cations. The proposed substitution is therefore:

$$H_3As^{V}O_4(aq) + 2\,SiO_4^{-4} \leftrightarrow \square H_3O_4^{-5} + As^{V}O_4^{-3} + 2\,SiO_2(aq)$$

(where $\square$ denotes defect). As silica activity is decreased in the fluid, the fluid will tend to conserve silica and drive this reaction to the right. Hydrogarnet substitution is well documented in many other studies (see Amthauer and Rossman 1998; Rossman and Aines 1991; and references therein). This substitution has also been shown to be favored by a fairly low reaction energy of only 98 kJ/mol (Wright et al. 1994). This mechanism may explain how As is incorporated in other skarn garnets such as at Connemara, and may even be a general explanation of how other

highly charged cations such as tungsten are accommodated in the garnet structure. Sufficient hydroxyl is contained within the structure as indicated by FTIR analysis to make this proposed substitution possible. In any case, the presence of tetrahedral As is clearly proven by this work. Further work will be necessary before the mechanism by which charge balance is maintained can be stated definitively. Because of the highly zoned nature of this garnet, spatially resolved spectroscopy will be critical to fully resolving its chemistry and structure.

We believe that the data presented here may play an important role in interpreting the geochemistry of arsenic in hydrothermal systems dominated by silicate mineral formation as opposed to the sulfide-rich systems typically associated with arsenic deposition. When the system is oxidizing enough to stabilize As^{5+}, in some cases related to boiling, vapor transport and incorporation of arsenate in rapidly precipitated garnet as a substitute for tetrahedral silica may be more common than previously recognized. Indeed, this type of substitution is also apparently important in arsenic recycling from the down-going slab back into the crust as observed by Hattori et al. (2005) and should not be neglected when trying to understand arsenic mobility—a critical geochemical and environmental problem.

Acknowledgments

Support for this study was provided by EPSRC through a research grant (GR/S30207/01) to D.A. Polya, J.R. Lloyd, D.J. Vaughan, and R.A. Wogelius, and CCLRC for a synchrotron beamtime award (42/217) to D.A. Polya and A.G. Gault. We thank Bob Bilsborrow of Daresbury Laboratory for his assistance during data collection. R.A.W. would like to thank Bjorn Jamtveit for generously supplying these samples in time for our beam allocation period. Thanks also go to Roger Speak, Assos Charalambos, John Waters, and Dave Plant for assistance with the supplementary chemical analyses. Comments from G. Diego Gatta (Associate Editor), Simona Quartieri, and an anonymous reviewer helped improve the manuscript.

References cited

Amthauer, G. and Rossman, G.R. (1998) The hydrous component in andradite garnet. American Mineralogist, 83, 835–840.

Binsted, N. (1992) Constrained and restrained refinement in EXAFS data analysis with curved wave theory. Biochemistry, 31, 12117–12125.

——— (1998) EXCURV98, computer program. CCLRC Daresbury Laboratory, U.K.

Bostick, B.C. and Fendorf, S. (2003) Arsenite sorption on troilite (FeS) and pyrite (FeS_2). Geochimica et Cosmochimica Acta, 67, 909–921.

Cances, B., Juillot, F., Morin, G., Laperche, V., Alvarez, L., Proux, O., Hazemann, J.L., Brown, G.E., and Calas, G. (2005) XAS evidence of As(V) association with iron oxyhydroxides in a contaminated soil at a former arsenical pesticide processing plant. Environmental Science and Technology, 39, 9398–9405.

Coker, V.S., Gault, A.G., Pearce, C.L., van der Laan, G., Telling, N.D., Charnock, J.M., Polya, D.A., and Lloyd, J.R. (2006) XAS and XMCD evidence for species-dependent partitioning of arsenic during microbial reduction of ferrihydrite to magnetite. Environmental Science and Technology, 40, 7745–7750.

Donnay, G. and Allmann, R. (1968) Si_3O_{10} Groups in crystal structure of ardennite. Acta Crystallographica B: Structural Crystallography and Crystal Chemistry, 24, 845.

Esson, J., Stevens, R.H., and Vincent, E.A. (1965) Aspects of geochemistry of arsenic and antimony exemplified by Skaergaard intrusion. Mineralogical Magazine, 35, 88–107.

Farquhar, M.L., Charnock, J.M., Livens, F.R., and Vaughan, D.J. (2002) Mechanisms of arsenic uptake from aqueous solution by interaction with goethite, lepidocrocite, mackinawite, and pyrite: An X-ray absorption spectroscopy study. Environmental Science and Technology, 36, 1757–1762.

Filatov, S.K., Krivovichev, S.V., Burns, P.C., and Vergasova, L.P. (2004) Crystal structure of filatovite, $K[(Al,Zn)_2(As,Si)_2O_8]$, the first arsenate of the feldspar group. European Journal of Mineralogy, 16, 537–543.

Gault, A.G., Polya, D.A., Charnock, J.M., Islam, F.S., Lloyd, J.R., and Chatterjee, D. (2003a) Preliminary EXAFS studies of solid phase speciation of As in a West Bengali sediment. Mineralogical Magazine, 67, 1183–1191.

Gault, A.G., Polya, D.A., Lythgoe, P.R., Farquhar, M.L., Charnock, J.M., and Wogelius, R.A. (2003b) Arsenic speciation in surface waters and sediments in a contaminated waterway: an IC-ICP-MS and XAS based study. Applied Geochemistry, 18, 1387–1397.

Gault, A.G., Cooke, D.R., Townsend, A.T., Charnock, J.M., and Polya, D.A. (2005) Mechanisms of arsenic attenuation in acid mine drainage from Mount Bischoff western Tasmania. Science of the Total Environment, 345, 219–228.

Gramaccioli, C.M., Liborio, G., and Pilati, T. (1981) Structure of medaite, $Mn_6[VSi_5O_{18}(OH)]$—the presence of a new kind of heteropolysilicate anion. Acta Crystallographica B, Structural Science, 37, 1972–1978.

Grime, G.W., Watt, F., Wogelius, R.A., and Jamtveit, B. (1993). Processing microPIXE linescan data—studies of arsenic zoning in skarn garnets. Nuclear Instruments and Methods in Physics Research B—Beam Interactions with Materials and Atoms, B77, 410–414.

Gurman, S.J., Binsted, N., and Ross, I. (1984) A rapid, exact curved-wave theory for EXAFS calculations. Journal of Physics C—Solid State Physics, 17, 143–151.

Hattori, K., Takahashi, Y., Guillot, S., and Johanson, B. (2005). Occurrence of arsenic (V) in forearc mantle serpentinites based on X-ray absorption spectroscopy study. Geochimica et Cosmochimica Acta, 69, 5585–5596.

Hedin, L. and Lundqvist, S. (1969) Effects of electron-electron and electron-phonon interactions on the one-electron states of solids. Solid State Physics, 23, 1–181.

Hudson-Edwards, K.A., Jamieson, H.E., Charnock, J.M., and Macklin, M.G. (2005) Arsenic speciation in waters and sediment of ephemeral floodplain pools, Rios Agrio-Guadiamar, Aznalcollar, Spain. Chemical Geology, 219, 175–192.

Jamtveit, B. (1991) Oscillatory zonation patterns in hydrothermal grossular-andradite garnet—nonlinear dynamics in regions of immiscibility. American Mineralogist, 76, 1319–1327.

Jamtveit, B., Wogelius, R.A., and Fraser, D.G. (1993) Zonation patterns of skarn garnets: Records of hydrothermal system evolution. Geology, 21, 113–116.

La Force, M.J., Hansel, C.M., and Fendorf, S. (2000) Arsenic speciation, seasonal transformations, and co-distribution with iron in a mine waste-influenced palustrine emergent wetland. Environmental Science and Technology, 34, 3937–3943.

Morin, G. and Calas, G. (2006) Arsenic in soils, mine tailings, and former industrial sites. Elements, 2, 97–101.

Morin, G., Juillot, F., Casiot, C., Bruneel, O., Personne, J.C., Elbaz-Poulichet, F., Leblanc, M., Ildefonse, P., and Calas, G. (2003) Bacterial formation of tooeleite and mixed Arsenic(III) or Arsenic(V)-Iron(III) gels in the carnoulbs acid mine drainage, France. A XANES, XRD, and SEM study. Environmental Science and Technology, 37, 1705–1712.

Paktunc, D., Foster, A., and Laflamme, G. (2003) Speciation and characterization of arsenic in Ketza River mine tailings using X-ray absorption spectroscopy. Environmental Science and Technology, 37, 2067–2074.

Paktunc, D., Foster, A., Heald, S., and Laflamme, G. (2004) Speciation and characterization of arsenic in gold ores and cyanidation tailings using X-ray absorption spectroscopy. Geochimica et Cosmochimica Acta, 68, 969–983.

Pascua, C., Charnock, J., Polya, D.A., Sato, T., Yokoyama, S., and Minato, M. (2005) Arsenic-bearing smectite from the geothermal environment. Mineralogical Magazine, 69, 897–906.

Rossman, G.R. and Aines, R.D. (1991) The hydrous components in garnets: grossular-hydrogrossular. American Mineralogist, 76, 1153–1164.

Rowland, H.A.L., Gault, A.G., Charnock, J.M., and Polya, D.A. (2005) Preservation and XANES determination of the oxidation state of solid-phase arsenic in shallow sedimentary aquifers in Bengal and Cambodia. Mineralogical Magazine, 69, 825–839.

Savage, K.S., Bird, D.K., and O'Day, P.A. (2005) Arsenic speciation in synthetic jarosite. Chemical Geology, 215, 473–498.

Sherman, D.M. and Randall, S.R. (2003) Surface complexation of arsenic(V) to iron(III) (hydr)oxides: Structural mechanism from ab initio molecular geometries and EXAFS spectroscopy. Geochimica et Cosmochimica Acta, 67, 4223–4230.

Takeuchi, Y., Haga, N., Umizu, S., and Sato, G. (1982) The Derivative Structure of Silicate Garnets in Grandite. Zeitschrift fur Kristallographie, 158, 53–99.

Thoral, S., Rose, J., Garnier, J.M., Van Geen, A., Refait, P., Traverse, A., Fonda, E., Nahon, D., and Bottero, J.Y. (2005) XAS study of iron and arsenic speciation during Fe(II) oxidation in the presence of As(III). Environmental Science and Technology 39, 9478–9485.

Tournassat, C., Charlet, L., Bosbach, D., and Manceau, A. (2002) Arsenic(III) oxidation by birnessite and precipitation of manganese(II) arsenate. Environmental Science and Technology, 36, 493–500.

Wright, K., Freer, R., and Catlow, C.R.A. (1994) The energetics and structure of the hydrogarnet defect in grossular: a computer simulation study. Physics and Chemistry of Minerals, 20, 500–503.

Zhang, Z. and Saxena, S.K. (1991) Thermodynamic properties of andradite and application to skarn with coexisting andradite and hedenbergite. Contributions to Mineralogy and Petrology, 107, 255–263.

Manuscript received December 19, 2006
Manuscript accepted July 3, 2007
Manuscript handled by G. Diego Gatta